

Improved design of a multi-stage continuous-resistance trim for minimum energy loss in control valves.

ASIM, T., OLIVEIRA, A., CHARLTON, M. and MISHRA, R.

2019



Improved design of a multi-stage continuous-resistance trim for minimum energy loss in control valves



Taimoor Asim ^{a,*}, Antonio Oliveira ^a, Matthew Charlton ^b, Rakesh Mishra ^a

^a School of Computing & Engineering, University of Huddersfield, Queensgate, Huddersfield HD1 3DH, UK

^b Weir Valves & Controls UK Ltd, Britannia House, Elland HX5 9JR, UK

ARTICLE INFO

Article history:

Received 22 December 2017

Received in revised form

26 February 2019

Accepted 6 March 2019

Available online 9 March 2019

Keywords:

Control valves

Computational fluid dynamics

Continuous-resistance trims

Local flow behaviour

Pressure drop

ABSTRACT

Control valves used in energy systems are often integrated with trims having well designed flow paths to regulate fluid flow. These trims, known as multi-stage continuous-resistance trims, comprise of staggered arrangement of circular cylinders enabling pressure drop reduction in controlled stages. The trim design process currently used doesn't ensure good local flow characteristics and relies almost entirely on the global performance indicators. The existing design largely ignores the effects of geometrical features of the trim, resulting in severe performance issues locally. In the present investigation, unique geometry-dependant local flow parameters have been analysed, using Computational Fluid Dynamics, and integrated with the global performance indicators to develop an improved trim design. Novel geometry and flow based parameters have been developed that uniquely relate the local flow behaviour within the trims to their corresponding geometrical parameters. It has been observed that the change in geometrical parameters of the trim significantly affects trim's performance, for example, reduction in the cylinders' dimensions, under same operating conditions, reduces the normalised pressure drop, flow velocity and energy by 28.4%, 26.8% and 37.9% respectively. The work highlights the need for modification in existing trim design methodology.

© 2019 The Authors. Published by Elsevier Ltd. This is an open access article under the CC BY license (<http://creativecommons.org/licenses/by/4.0/>).

1. Introduction

Control valves are used for flow control in various integrated energy systems, ranging from conventional power plants, to nuclear and oil and gas systems. A control valve consists of a number of key components, such as the valve's pressure envelope (containing the valve body, bonnet, bolts etc), a stem and an actuator, as shown in Fig. 1(a and b) [1]. An essential component of a control valve is a trim assembly (containing the plug, seat, cage/guide etc) that is designed to regulate the flow and avoid/minimise cavitation, vibrations and noise within the valve [2]. There are many types of trims commercially available, and the one used for higher pressure drop applications are commonly known as multi-stage continuous-resistance trims, which consist of staggered arrangement of circular cylinders (Fig. 1(c)) [3]. The control valve trims are carefully designed to ensure that the flow propagates in a controlled manner

[4]. The geometry of trim's flow paths can have variety of shapes including that of a converging-diverging duct [5]. The flow propagation along the flow paths may result in flashing/cavitation and different stages [6]. Depending on the area available for the flow, the supersonic conditions can also recur within the complex flow geometry [7]. The above discussion indicates that the geometrical features of the trim have a considerable effect on the flow field characteristics, as well as the operational characteristics of a control valve. The overall size (inner and outer diameters) of the trim is generally dictated by the design specifications of the valve and the process conditions that the valve is designed to operate in.

The primary design parameter of a control valve is its flow capacity ($Cv_{\text{Control-Valve}}$) [9]. The flow capacity of a control valve depends on the flow capacity of the trim (Cv_{Trim}), as given below [10]:

$$\frac{1}{Cv_{\text{Control-Valve}}^2} \propto \frac{1}{Cv_{\text{Trim}}^2} \quad (1)$$

and:

* Corresponding author.

E-mail addresses: t.asim@hud.ac.uk (T. Asim), Antonio.Oliveira2@hud.ac.uk (A. Oliveira), Matthew.Charlton@weirgroup.com (M. Charlton), r.mishra@hud.ac.uk (R. Mishra).

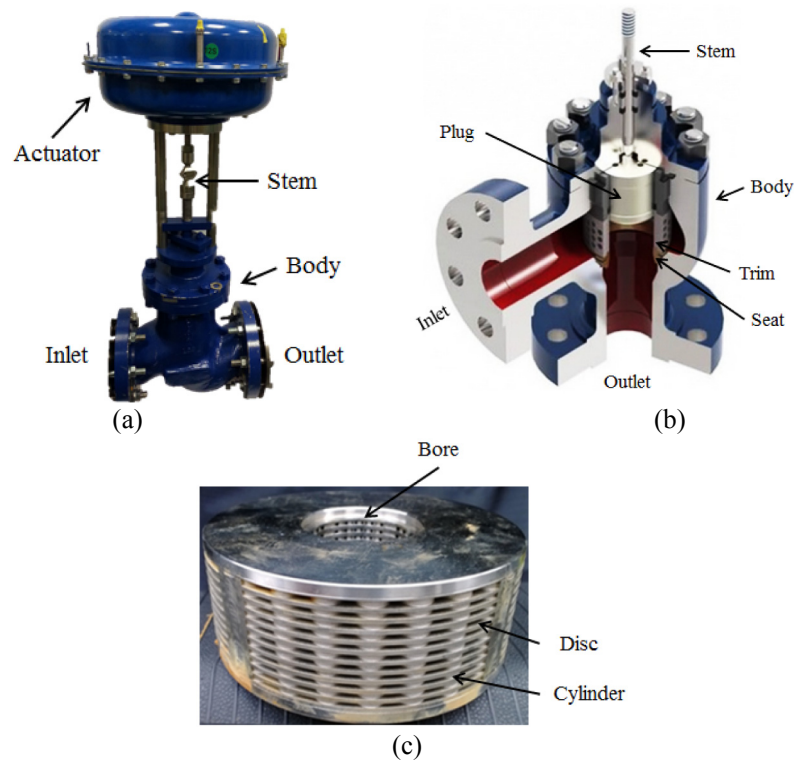


Fig. 1. Components of a control valve (a) valve and the actuator (b) valve body with the trim [8] (c) the trim.

$$Cv_{Trim} \propto \frac{Q_{Trim}}{\sqrt{\Delta P_{Trim}}} \quad (2)$$

where Cv_{Trim} is the flow capacity of the trim. In equation (2), Q_{Trim} and ΔP_{Trim} are the flow rate (in m^3/hr) and the overall/global pressure drop (in kPa) across the trim. The sizing equations for multi-stage control valves use the above mentioned parameters for designing a control valve trim [11]. It can be seen in equations (1) and (2) that the design of the trim (and the control valve) is explicitly dependent on global flow parameters. The typical design process involves providing flow area to maintain the Cv value through well controlled expansion. However, the flow field within the trim is expected to be highly complex and three-dimensional in nature, which can significantly affect the trim's local flow effectiveness. This aspect is not included in the conventional design of the trims (and the control valve). In the present study, an attempt has been made to correlate the local flow features of the trims with their global performance indicators, as well as local geometrical features. This in-turn will improve the design of these trims enabling better flow control at local level.

Recently, some studies have been conducted to analyse the local flow behaviour within multi-stage continuous-resistance trims. Green et al. [12] carried out extensive experimental and Computational Fluid Dynamics (CFD) based investigations in order to better understand the complex flow behaviour within a control valve, integrated with a multi-stage continuous-resistance trims. In these investigations, a commonly used globe-type control valve has been used. The operating pressures were in the range of 2–5 bar. It has been reported that $Cv_{Control-Valve}$ and Cv_{Trim} are independent of the flow rate passing through them. The results have been compared against the experimental data, however, significant differences have been observed amongst them. Furthermore, Green

et al. [13] has reported that numerically computed Cv_{Trim} has been shown to be 25% higher than the experimentally computed Cv_{Trim} . The possible reason for this discrepancy in the numerical results has been attributed to the fact that only a quarter of a disc of the trim has been considered, which is a significant simplification as the flow is expected to be highly three dimensional in the trim. Klas et al. [14] have clearly stated in their numerical study of a comparison between 2D and 3D modelling of the control valves that 2D numerical modelling fails to account for the backflow in the valve, and hence, the numerical results based on the 2D modelling cannot be relied on. The study also pointed out that the velocity field within the 2D control valve varied significantly as compared to its 3D counterpart. This has led Asim et al. [15], Asim et al. [16] and Antonio et al. [17] to study the local flow behaviour within a control valve, and multi-stage continuous-resistance trims, using a 3D numerical modelling approach. It has been reported that although $Cv_{Control-Valve}$ and Cv_{Trim} are independent of the flow conditions, as the valve opening position increases, both these flow capacities also increase [15]. The flow conditions considered in these studies, experimentally, are the same as considered by Green et al. [12]; however, the numerical investigations have been carried out in the range of 10–100 bar operating pressure, which corresponds to severe service applications. Asim et al. [16] have reported that there are significant pressure and velocity variations observed within the trim and hence, a critical local flow analysis is essential to develop better trim designs. It has been observed that the flow paths (area between the cylinders) are prone to cavitation as the local static pressure here may drop below the vapour pressure line. Antonio [17] carried out further local flow analyses within the trim, under similar flow conditions as that of Asim et al. [15], reporting that the local flow behaviour is non-uniform not only in the radial direction of the trim (i.e. fluid flowing inwards/outwards), but it is also highly complex in the different discs of the trim (vertically). Hence, the

cavitation behaviour can change between the different discs of the trim. Although the aforementioned studies analysed the complex flow behaviour within the trim, no attempts were made to include the correlations quantifying the local flow behaviour into the design of the trims and the control valves.

Wang et al. [18] carried out extensive numerical investigations on the flow structure within bell-shaped control valves. These investigations have been performed at valve pressure ratios of 0.95 to 0.05, and valve's open ratio of 50%–2%. It has been reported that the flow within the control valve can be categorised into an annular attachment flow (jet flow) and a central detachment flow (back flow), separated by a pair-vortex. These flow regimes are significantly affected by the valve's pressure and open ratios; higher ratios resulted in centrally detached flow, while lower ratios resulted in annular attached flow. It has been further reported that the primary reason for the change in the flow regimes within the control valve is the Coanda effect. Although a detailed local flow analysis has been presented, it has not been quantified and the observed flow behaviour has not been reflected in the design of the valve. Qiu et al. [19] performed numerical investigations on the effects of control valve's needle/stem speed on the cavitation behaviour of the valve. The operating conditions tested were in the range of 43–124 MPa of inlet pressure, and 2–50 MPa of outlet pressure. It has been reported that, under same operating conditions, increase in the spindle speed results in increase in the mass flow rate passing through the valve. This in-turn has been observed to decrease the cavitation within the valve. This information is very useful in terms of valve and trim design; however, Qiu et al. [19] have not formulated a strategy to implement spindle speed as a parameter for the design and operation of the valve. Kong et al. [20] took the analysis of the internal flow field within control valves further, and applied flow field decomposition, and its reconstruction, for modelling the hydrodynamic characteristics of a valve. Numerical investigations have been carried out at flow rates in the range of 20–250 l/min. Using Proper Orthogonal Decomposition (POD), the local flow behaviour within a valve has been reconstructed with 99.53% accuracy using only 10 high energy modes. The error between the reconstructed and actual pressure field has been reported to be below 5%. The results presented in the study are very useful and a way needs to be found to integrate the outcomes of this analysis into the design of a control valve. However, this aspect has not been considered. In the present study, extensive local flow field analyses have been carried out within the control valve and the trim, using a range of different techniques/parameters. This information has then been integrated with the global performance indicators of the trim to develop a novel design that takes care of local flow behaviour, as well as the global performance indicators of the trim.

The local flow behaviour within a multi-stage continuous-resistance trim is substantially affected by the geometrical parameters of the trim, which are in an ideal sense, the output of the design process. This indicates that to achieve pre-determined local flow behaviour, and overall performance characteristics of the control valve and the trim, there must be a direct method to calculate geometric dimensions of the trim. Recent studies have, to some extent, quantified the effects of various geometrical dimensions/shapes on the hydrodynamic behaviour of the trim/valve; however, this has not been used to develop a more sophisticated trim/valve design. For example, after Morton's [21] concept design of a multi-stage continuous-resistance trim, based on X shaped flow paths rather than + shaped flow paths, Asim [22] analysed various geometrical configurations suggested by Morton [21] using experimental and advanced numerical techniques. The operating range of these investigations is the same as considered by Asim et al. [15] and Antonio [17]. The trim's geometrical variations considered were the overall size (outer diameter), number of rows

of cylinders in a disc and the shape of end rows (semi-circular). These investigations have shown that $C_{V_{Trim}}$ decreases by 25.2% as the size of trim and the number of rows of cylinders increases from 5 to 7. Similarly, semi-circular cylinders in the end rows of the trim, as compared to circular cylinders, resulted in $C_{V_{Trim}}$ reduction (by 5%) due to flow separation. However, no attempt was made to integrate these results into the design of the trim. Charlton [23] has further analysed the effects of the manufacturing methods on the trim design by comparing trims manufactured using Electron Discharge Machining (EDM) and Selective Laser Melting (SLM). It has been shown that although EDM based multi-stage continuous-resistance trims are geometrically superior in design, the relative cost of SLM based trims make them more preferable for commercial viability [23]. Based on this information, several SLM based concept trims were designed by Charlton et al. [24], based on manufacturing experience, to enhance the flow capacity. These concept trims used thin wall and mirror body features to produce complex flow paths, rather than a standard lofted cut. Configurations such as ridged, wavy, arced and tear-drop shaped end flow paths were numerically tested and analysed, at the same operating conditions as in Asim [22]. The results show that, generally, the flow path area has a significant impact on the performance of the trim i.e. increased flow path area generally increases $C_{V_{Trim}}$ and vice versa. However, the trim consisting of tear-drop shaped end flow paths showed 9.7% improvement in performance, compared to a like-for-like trim design. The aforementioned studies included parametric design investigations but the outcomes were not integrated into the design of the trims in order to improve it.

Lisowski and Filo [25] carried out wide-ranging CFD based investigations on the hydrodynamic characteristics of a control valve. Various design modifications to the valve's spool geometry were employed in order to enhance the global performance indicators of the valve and to reduce the forces acting on the spool. These geometrical modifications included circular/triangular openings and introduction of a number of notches/under-cuts in the vicinity of the spool. Lisowski et al. [26] carried out numerical testing at a Reynolds number range of 300–2500. Based on the local flow behaviour within the control valve, it has been shown that the triangular openings increased the proportional operating range of the valve by 40%, while the use of 2 notches reduced the radial forces acting on the spool by 102%. This clearly shows that the shape of flow paths has a significant influence on the hydrodynamic behaviour of the valve; however, these findings have not been used to modify the existing design for control valves. Sun et al. [27] numerically investigated the effects of flow path geometry, considering the surface roughness effects, on the flow capacity of a valve. The operating conditions considered were Q_{max} in the range of 500–2500 m³/h, where Q_{max} is the maximum flow rate passing through the valve. It has been reported that the flow path geometry has significant influence on the global performance indicators of the valve. It has been stated that the surface roughness can vary the flow coefficient of the valve by 17%, on average, while it can be even higher at lower valve opening positions. An attempt has been made to correlate the geometric parameters of the valve with the global performance indicators. For this purpose, a semi-empirical expression has been developed for the pressure drop across the valve that takes into account the effects of surface roughness. However, there are two serious issues with the developed correlation. The first issue is that the developed correlation is not dimensionally homogeneous; pressure (Pa = kg/m.sec²) has significantly different units than roughness height (m). The other issue is that some terms in the correlation are a function of flow velocity, which has been specified, implicitly, as the inlet boundary condition.

Similar to Sun et al. [27], Jin et al. [28] carried out extensive

numerical investigations on the effects of core/stem's diameter and displacement on the pressure force acting on it, hence analysing the effects of flow path geometry on the valve's performance. These investigations have been carried out at flow velocities of 1.5 m/sec, 3.5 m/sec and 5.5 m/sec, while core diameters of 2–16 mm were considered. Moreover, the core displacements of 5–35 mm were used to carry out local flow field analysis, using flow and energy loss coefficients as the parameters. The energy loss parameter considered in this study is actually non-dimensional pressure drop. A more accurate energy loss parameter has been considered for analysis in the present study (in section 8.0). It has been reported by Jin et al. [28] that as the core diameter increases, the flow coefficients increases, while the loss coefficient decreases, which seems logical. Based on the numerical results, a number of correlations have been developed for the pressure forces acting on the core under varying flow conditions. Again, as seen in case of Sun et al. [27], these correlations are not dimensionally homogeneous, equating the flow velocity to the forces. Moreover, these correlations cannot be used explicitly in the design of a valve as the flow coefficient term is missing from these correlations. In the present study however, a novel trim design has been proposed and developed that explicitly relates the geometrical features of a control valve components to its design parameters.

The aforementioned literature suggests that the current literature lacks detailed information about the flow mechanics of the valve at local level, and its effects on global flow performance indicators of the valve. This results in limited information to make suitable changes in the design for smooth operation of the valve under diverse flow conditions. In the present investigation, the following novel elements have been addressed:

1. The inability of global performance indicators used in the design process to ensure satisfactory local flow characteristics over a wide range of operating conditions.
2. Development of novel parameters to quantify local and global flow characteristics.
3. Development of a novel parameter based on the local geometric features of the trim.
4. Developing an improved design of multi-stage continuous-resistance control valve trims that takes into account the local flow characteristics and geometric parameters.

In order to achieve the aforementioned aims, the study makes extensive use of a range of techniques, such as numerical (CFD), experimental (flow loop), statistical (Taguchi) etc. In the next section, the details of the numerical methodology employed have been discussed in detail.

2. Numerical modelling of the control valve

The numerical modelling of the multi-stage continuous-resistance trim and control valve has been carried out using Ansys 17.0 in order to establish the relationship between the local flow behaviour and the global performance indicators. The CFD based numerical modelling comprises of three stages i.e. pre-processing, solver setup and post-processing [29]. Pre-processing is further divided into the flow domain geometry creation and its meshing, and into solver setup, which includes the specification of boundary conditions, material properties, turbulence modelling, convergence criteria, initial solution etc. All these aspects need special consideration for flow through complex geometries [30]. Post-processing involves the analysis of CFD data obtained and for displaying flow features in a complex geometry, the choice of planes and the flow variables to be analysed need special consideration [31].

2.1. Geometry of the control valve

The geometry of the control valve, installed with the baseline model of the trim, is shown in Fig. 2. This model of the control valve is manufactured by the industrial collaborator and enjoys a large presence in process applications. The present work has been carried out in order to improve the current design, based on extensive investigations on the local flow features through the use of computation fluid dynamics, which are difficult to obtain from conventional experimental methods. It can be seen in Fig. 2(a) that D is the diameter of the valve's inlet and outlet sections. In accordance with BS EN 60534-2-5 [11], the inlet and outlet sections of the valve are connected to pipe sections (having same diameter). The lengths of these pipe sections (i.e. inlet and outlet sections) are $2D$ and $6D$ respectively. The geometrical characteristics of the trim, shown in the Fig. 2(b), depict that each disc of the trim comprises of four quarters, where each quarter further comprises of rows of circular cylinders. In the present study, the trim that has been considered for analysis, consists of five rows of cylinders. To facilitate numerical analysis, the outermost row is termed as row 1 and the inner most row is named as row 5. The fluid flows from row 1 to row 5 in the present study, as the flow is over the trim. The diameters of the cylinders in a particular row are constant, and are represented as d_1 for row 1, to d_5 for row 5. The radii, from the centre of the trim, to the centre of each row, are termed as r_1 to r_5 . It must be noted that $d_1 > d_2 > d_3 > d_4 > d_5$ in order to offer area expansion to the flow, to ensure systematic pressure reduction.

2.2. Meshing of the flow domain

The meshing of the flow domain is an essential step in CFD modelling. The meshing process ensures the breakdown of the flow domain into smaller parts, where each part is called a mesh element. The size of mesh elements affects the accuracy of flow near the regions of high flow velocity gradients [32]. For accurate prediction of the local flow behaviour in control valves, the flow domain should be broken down into a large number of mesh elements (millions in case of 3D problems). The same has been carried out in the present study by controlling the mesh element sizing [33]. The minimum mesh element size used in the present investigation is 0.35 mm, while the maximum size used is 3 mm. This has resulted in 5.3 million mesh elements within the valve and the trim, as shown in Fig. 3. This mesh corresponds to a mesh density of 445.6 elements per cm^3 . It can be further seen in Fig. 3 that two different types of mesh elements have been incorporated within the flow domain considered i.e. hexahedral and tetrahedral mesh elements. Hexahedral mesh elements have been used in the regions where the geometry is relatively simple and symmetric (like in the inlet and outlet pipes), while the tetrahedral elements have been used in the areas of high geometric complexities (like in the valve and the trim). The choice of the shape of the mesh elements is further dictated by the symmetry in the flow; for symmetric flows, hexahedral mesh elements are preferred, while for highly complex flows, tetrahedral elements provide accurate results [34]. It has been shown in section 3.0 that the resulting mesh is capable of accurately predicting the flow parameters within the valve and the trim.

In order to address the third aim of the present study i.e. quantifying the effects of geometrical features on the local and global flow characteristics within the trim and the valve, a more stringent control is required to mesh the small areas available for the flow to take place within the different rows of the trim, and which are different in different rows of the trim. Hence, a technique based on Proximity and Curvature of the flow domain walls (such as cylinders etc) has been used to manage the mesh elements within

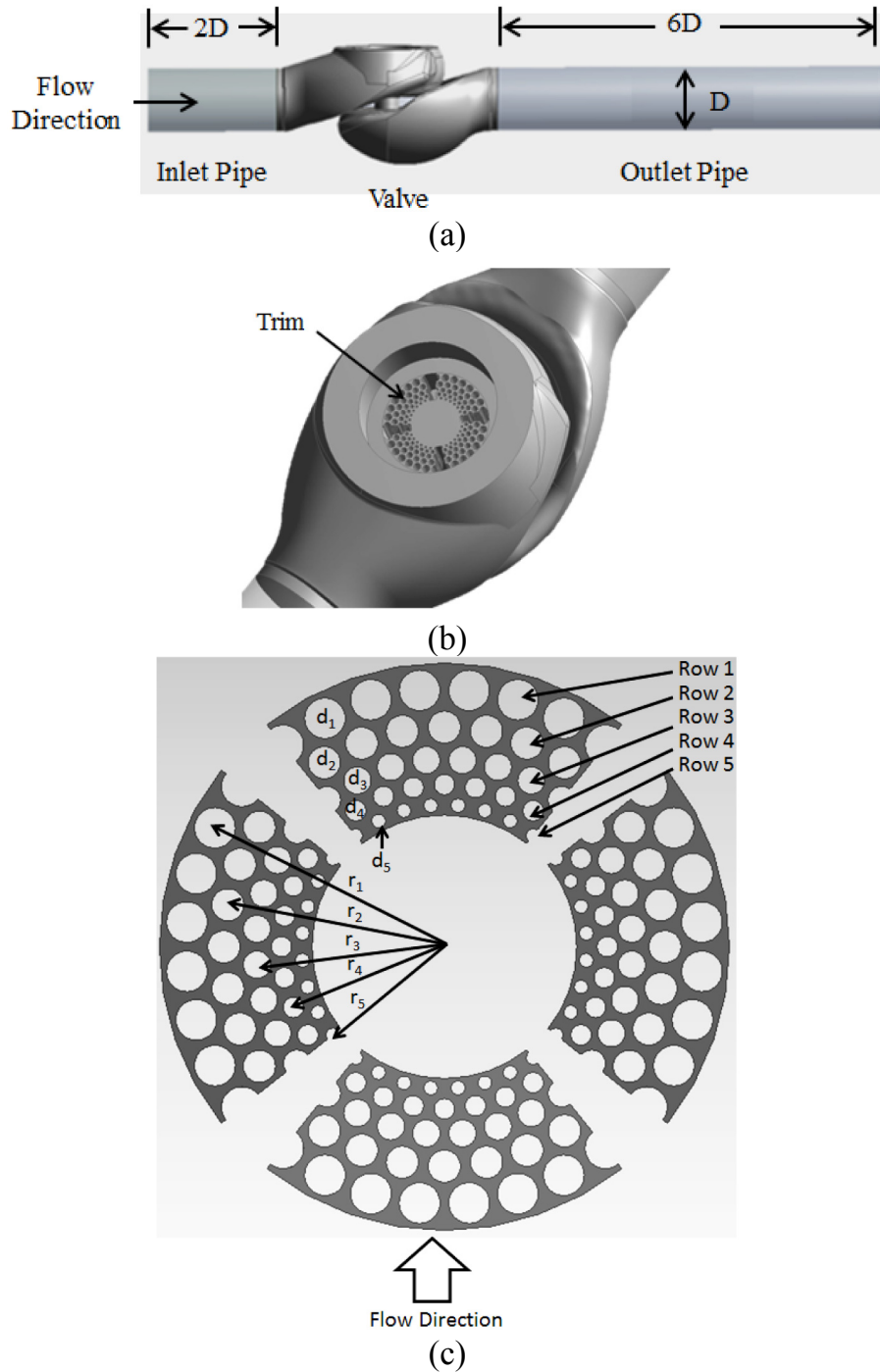


Fig. 2. The geometry of the control valve (a) flow domain (b) trim (c) geometrical characteristics of the trim.

the trim [35]. Further ensuring the accurate prediction of the flow related parameters in the near-wall regions, especially around the cylinders of the trim; additional layers of hexahedral elements (two for each cylinder) have been created with a specific growth rate (of 20%). These near-wall mesh element layers can be seen in Fig. 3. The mesh quality parameters, based on the mesh controls mentioned specified for 5.3 million elements mesh, is summarised in Table 1. It can be seen that all the average values of all the quality parameter indicate that this particular mesh is appropriate for further analysis.

2.3. Boundary conditions and material properties

It is an established fact that the flow capacity of a control valve trim is independent of the flow rate passing through it [12]. In the present study, the inlet boundary of the flow domain has been specified with a constant mass flow rate of 12.51 kg/s based on the recommendations stated in BS EN 60534-2 [2]. This mass flow rate value is the same to the value at which the experiments have been carried out in the present study (discussed in section 4.0). The outlet boundary of the flow domain has been modelled as pressure

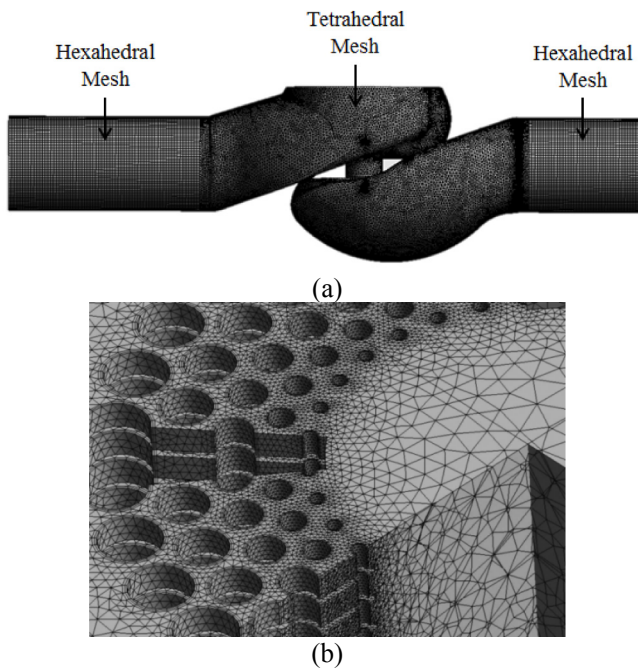


Fig. 3. Meshing of the flow domain (a) flow domain (b) trim.

Table 1
Mesh quality parameters.

Quality Parameter	Average Value
Element quality	0.78
Aspect ratio	2.19
Orthogonality	0.88
Skewness	0.20

outlet with a total gauge pressure of 0Pa i.e. atmospheric pressure. Moreover, turbulence intensity of 5% has been specified at both the inlet and outlet boundaries of the flow domain. All the walls in the flow domain (like cylinders, valve body etc.) have been modelled as no-slip walls, ensuring that there is no slip (velocity difference) between the wall and fluid velocity at the wall. A summary of the boundary conditions specified in the present study is presented in Table 2. Moreover, the fluid considered for both numerical and experimental testing of the valve and trim is water. The optimisation methodology developed in the current study may be used with other incompressible fluids as well, although the exact geometric changes will depend on the fluid being used. For compressible fluids, additional investigations may be needed. The values of density and dynamic viscosity of water specified are 998.2 kg/m^3 and $0.001003 \text{ kg/m-sec}$ respectively.

2.4. Turbulence modelling

Control valves are used in those industrial applications where the fluid flow needs to be regulated. In such applications, the flow

Table 2
Boundary conditions.

Boundary	Type	Value
Inlet	Mass flow rate	12.51 kg/s
Outlet	Pressure	0 kPa (total, gauge)
Walls (valve and trim)	Stationary walls	No-slip

velocity is reasonably high, resulting in turbulent conditions. Based on the mass flow rate of 12.51 kg/s passing through the valve in the present study, the Reynolds number of the flow at the inlet of the flow domain has been calculated to be 1.5×10^5 which is well above the threshold value of turbulent flow. Moreover, while passing through the different sections of the valve and the trim, as the area available for the flow to take place decreases, the Reynolds number further increases, ensuring the flow to be turbulent throughout the flow domain.

There are different turbulence models that have been mentioned in the texts [36], and it is known that particular models are suitable for specific applications. It has been shown by Asim et al. [37] that the use of a two equation turbulence model, known as $k-\omega$ turbulence model, is preferable in case of internal flows. Here k refers to the turbulent kinetic energy while ω represents the turbulence dissipation rate. The $k-\omega$ turbulence model has two further variants i.e. the standard model and the Shear Stress Transport (SST) model [38]. In the present study, the SST model has been used to model turbulence in the flow because of its superiority in predicting complex flow features (like adverse pressure gradients) within valves and trims, as compared to the standard model [39]. Hence, in addition to the Reynolds averaged Navier-Stokes equations (RANS; for 3D flows), and the mass conservation equation, the equations of k and ω are also solved iteratively. An independent comparative study between SST- $k-\omega$ and standard $k-\epsilon$ turbulence model has been carried out, which has shown that while SST $k-\omega$ model under-predicts the static gauge pressure at the inlet of the flow domain by 5.2% (discussed in section 4.0 of this study), the widely used standard $k-\epsilon$ model over-predicted it by 18.7%. The use of appropriate turbulence model for multiphase flows in complex geometries requires special consideration. Pradhan et al. [40] developed measurement techniques for local fluctuations in the velocity field that may have impact on local turbulence in multiphase flows. Asim et al. [41] developed a comprehensive model for global flow characteristics in flow through complex geometries for multiphase flow applications.

2.5. Solver setup

The RANS equations have been discretised which requires pressure-velocity coupling for accurate prediction of pressure drop across the complex flow field [42]. For this purpose, a Semi Implicit Method for Pressure Linked Equations (SIMPLE) has been used that solves a pressure correction equation [43]. Similarly, for spatial discretisation of gradient (constructing cell-centred scalars), a Green-Gauss Node-based gradient evaluation has been used in the present study. 2nd order upwinding has been specified for the discretisation of momentum and turbulence parameters, in order to accurately predict the complex flow features within the valve and the trim. An independent comparative study between the 1st order and 2nd order discretisation schemes has been carried out. The study shows that while 2nd order schemes under-predicts the static gauge pressure at the inlet of the flow domain by 5.2% (discussed in section 4.0), the 1st order schemes under-predicted it by 6.7%. Hence, the 2nd order discretisation schemes are more suitable in case of control valves.

Convergence achieved through numerical techniques is a rather subjective matter, depending on the convergence criteria being specified. In the present study, the convergence of static gauge pressure at the inlet of the flow domain (in kPa) has been monitored throughout the iterative process of the pressure-based steady-state solver, as shown in Fig. 4. It can be seen that after the initial solver instabilities (first 100 iterations), the pressure at the inlet (P_{in}) gradually increases. Roughly after 1800 iterations of the solver, the inlet pressure values gets converged, which means

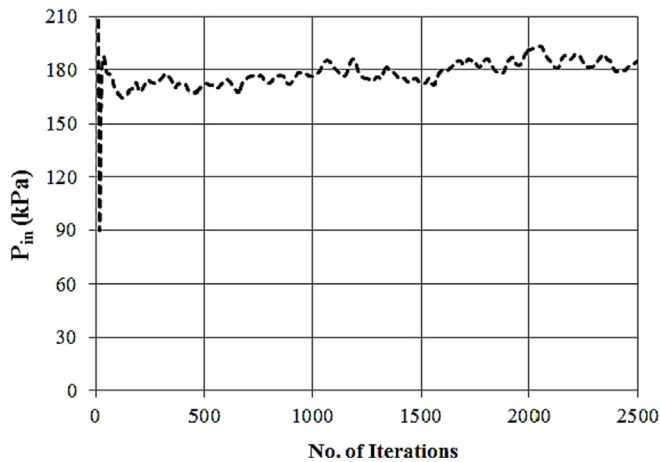


Fig. 4. Convergence of the solution.

that although there are variations in the inlet pressure values, these variations are cyclic with very small deviation from the mean value. Hence, all the numerical simulations conducted in the present study have been run for 2500 iterations.

3. Mesh independence and grid convergence studies

The process of determining the number of mesh elements required for an accurate numerical solution is called as Mesh Independence Testing. Without mesh independence testing, the validity of numerically predicted flow features remains uncertain. For this purpose, a number of meshing schemes have been developed [44]. A comparison of the flow parameters predicted using different mesh schemes indicate the appropriateness of number of mesh elements required to accurately predict the complex flow field. In the present study, apart from the already generated 5.3 million elements mesh, three more mesh schemes were used. These mesh schemes result in mesh element numbers of 3.4 million, 4.3 million and 6.5 million mesh elements for the three cases respectively. Inlet pressure (similar to Fig. 4) is recorded for each of these mesh schemes. The results corresponding to these cases are depicted in Fig. 5.

It can be seen that almost all the mesh schemes show the same trend i.e. gradual increase in the inlet pressure. The convergence in case of lesser number of elements is much quicker, however, the

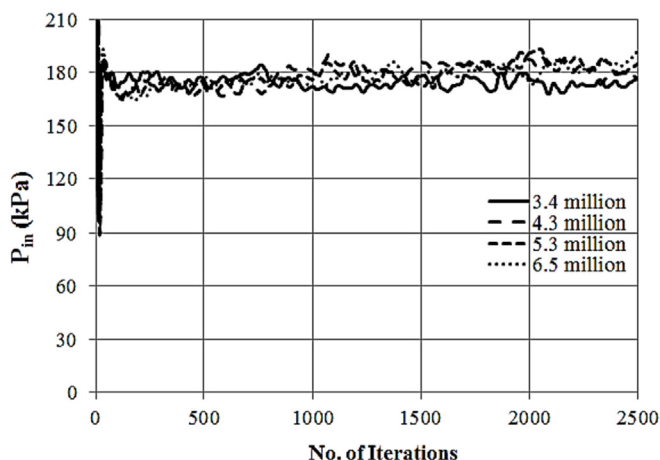


Fig. 5. Mesh independence testing results.

final pressure values are different. Hence, only the average P_{in} values for the last 500 iterations have been evaluated in Table 3.

It can be seen from Table 3 that the average inlet pressure value has increased when mesh elements have increased from 3.4 million to 5.3 million. There is a slight decrease in pressure values when mesh elements have increased from 5.3 million to 6.5 million. Furthermore, analysis of average P_{in} values shows that there is an increase of 5.1% in P_{in} value at 4.3 million mesh elements as compared to 3.4 million mesh elements. From 4.3 to 5.3 million mesh elements, this increase is 1.9%, and from 5.3 to 6.5 million mesh elements, the increase further reduces by only 0.9%.

A Grid Convergence Study (GCS) has been carried out in the present study to narrow down on the most appropriate mesh to be used for further investigations. As discussed earlier, 2nd order discretisation scheme has been used here; hence, the theoretical order to convergence is 2. The order of convergence of the numerically predicted results shown in Table 1 has been calculated to be 2.372. The difference between the theoretical and numerical order of convergences is due to a number of factors, such as solution, non-linearities, appropriateness of the turbulence model used, surface roughness effects in real-world etc. Based on Richardson extrapolation on 5.3 and 6.5 million element meshes [45], the estimated P_{in} value at zero grid spacing has been computed to be 182.9 kPa. This has been plotted as a dashed-line in Fig. 6, along with the numerically predicted P_{in} values at different mesh densities. It can be seen that the numerical solution tends to reach the estimated inlet pressure value.

Based on these results, Grid Convergence Index (GCI) has been computed for the different mesh schemes considered in the present study (Table 4). GCI between 6.5 and 5.3 million elements meshes has been calculated to be -0.26% , whereas, between 5.3 and 4.3 million elements meshes, GCI is 0.53% . Furthermore, GCI value between 4.3 and 3.4 million elements meshes has been computed to be 1.45% . Note that these GCI values have been computed based on a safety factor of 1.25, as suggested for more than three mesh schemes considered [45]. Based on the GCI values, the mesh with 5.3 million mesh elements has been considered to be capable of predicting the complex flow features within the valve and the trim with reasonable accuracy, and hence this mesh scheme has been chosen for carrying out further work in the present study.

4. Benchmark testing of the control valve

In numerical methods, the validation of numerical/mathematical models is of great importance for the legitimacy of the numerical results. Benchmarking consists of carrying out experiments in a controlled environment (laboratory based; same as specified in the numerical solver) and to evaluate the global performance indicators of the flow handling mechanical artefacts [46]. For benchmarking purposes, some special probes may need to be developed especially for complex flow and/or fluids [47]. Hence, in the present study, the same control valve and the trim, as used in the numerical work, have been experimentally tested for quantifying the variation of pressure across the valve against the flow rate. It must be noted that the differential pressure across the control

Table 3
Average P_{in} comparison.

(million)	(kPa)	(%)
No. of Mesh Elements	Average P_{in}	Difference in average P_{in}
3.4	172.8	–
4.3	181.6	5.1
5.3	184.9	1.9
6.5	183.3	0.9

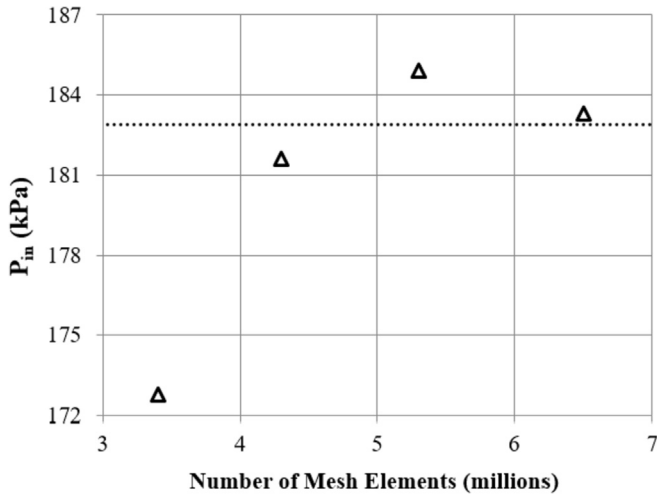


Fig. 6. Grid convergence study.

Table 4
Grid convergence index.

No. of Mesh Elements (million)	GCI
3.4	1.45
4.3	0.53
5.3	-0.26
6.5	

valve, as predicted from CFD, was 184.9 kPa (as mentioned in Table 3 corresponding to 5.3 million elements for an outlet pressure of 0 kPa).

A flow loop has been developed for hydrodynamic characterisation of the control valves. The schematic of the flow loop is shown in Fig. 7(a). The flow loop consists of a 1 m × 1 m × 1 m plastic tank that serves as the water reservoir. This tank is connected to a centrifugal pump via a Polyvinyl Chloride (PVC) pipe. The pump

housing is made of cast iron with an impeller of grade 14 cast iron. The shaft that connects the electric motor to the impeller is made of grade 316 stainless steel, and has a power of 24.1 kW at duty point. The electric motor has a rated power of 37 kW and a nominal speed of 2900 rpm. The rated voltage and maximum current of the motor are 3–400 V at 50 Hz and 65 A respectively. The pump delivers a head of 54.7 m and flow rate of 26.2ltr/sec at the duty point. The pump and the motor are connected to an inertia base made of four parts gravel, 2 parts sand and 1 part cement mixture. The 250 mm deep inertia base is fixed to the floor through four anti-vibration mounts, consisting of springs with a maximum deflection of 20 mm at optimum load conditions, where each mount can support up to 198.9 kg of point load. The pump with its base is shown in Fig. 7(b).

The centrifugal pump is connected to a full bore turbine flow meter, suitable for cold water applications. The self-cleaning synthetic resin based impeller rotates on stainless steel spindles that align with the pipe axis. The turbine flow meter can measure the flow rates in the range of 1.8–120 m³/h with a maximum pressure loss of 0.2% at maximum flow rate. The body of the flow meter is made of cast iron, as shown in Fig. 7(c). The turbine flow meter has been integrated into the flow loop to monitor the fluid flow rate passing through the loop. Further down the line, the control valve is installed with pressure tapplings placed 2D before and 6D after the valve as per the suggestions from standards. Four pressure tapplings are installed at each section to measure the average pressure within the pipeline. The pressure tapplings are connected to a differential pressure transducer that records the differential pressure across the control valve. The differential pressure transducer is based on piezo-resistive stainless steel sensors, as shown in Fig. 7(d). It has a pressure range of 20 mbar to 16 bar, with a supply of 12 V DC and output of 0–20 mA. The pressure transducer works in a temperature range of +5 to +125 °C, which is suitable for the experiments conducted in the present study. The accuracy of the transducer is ±0.5%. The differential pressure transducer used can measure up to 2.5 bar differential pressure, with an accuracy of ±0.5%. The differential pressure transducer feeds the current data to an AC-DC converter, where a calibration equation is used to calculate the

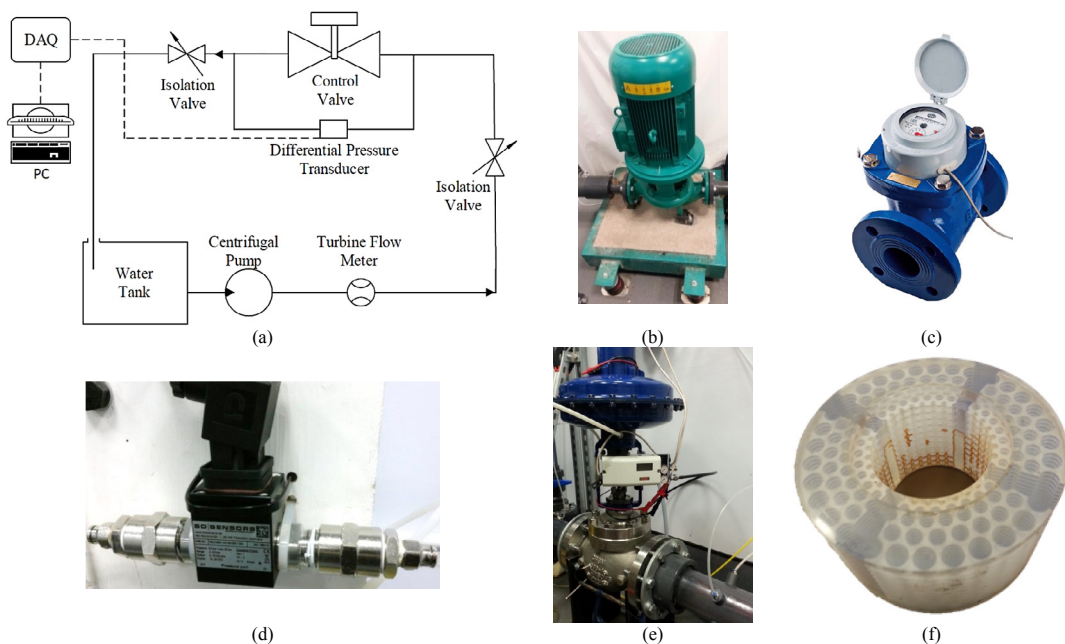


Fig. 7. Components of the flow loop (a) schematic (b) centrifugal pump (c) turbine flow meter (d) differential pressure transducer (e) control valve (f) baseline trim.

differential pressure across the control valve.

The control valve, as shown in Fig. 7(e), has a globe type body manufactured in A351 CF8M cast. As 80% of the control valves are pneumatically controlled by the actuators, the control valve used in the present study is fitted with a diaphragm based pneumatic actuator. The actuator is controlled by 4.5 bar gauge air supply, and is made of stainless steel. The body of the valve is globe type with ASME 300 rating. The trim sits within the valve body, on a seat. The trim/s used in the present study, as shown in Fig. 7(f), is made of a material known as TuskXC2700T using a 3D printing technique known as Stereolithography. A flow chart summarising the experimental procedures followed in the present investigation is presented in Fig. 8. The first step in the experimental testing of the control valve under consideration is to install the valve in the flow loop. Before starting the tests, the atmospheric pressure and water temperature need to be recorded in order to compute the density of water. In the present study, tests have been run at a constant flow rate of 45.12 m³/h as recommended in BS EN 60534-2 [2,9–11]. Inlet pressure (absolute), the flow rate of water and differential pressure across the control valve have been recorded.

The average differential pressure recorded across the valve from the different runs is 195.1 ± 0.97 kPa, which is 5.2% higher than the value that is numerically predicted, which is acceptable due to a number of variables affecting the experimental results, such as human error in precisely recording the data, geometrical imperfections in the valve and the trim, surface roughness of the real world valve etc. Based on these recorded values of flow rate and differential pressure, the flow capacity of the trim has been computed.

5. Hydrodynamic performance evaluation of the trim

In the present study, the trim that has been used for both experimental and numerical analyses will be referred to as the baseline trim. The local flow behaviour (variations in local pressure, local velocity etc) of this trim needs to be correlated to its global performance indicators (overall pressure drop, flow rate etc) in order to develop an improved design of multi-stage continuous-resistance trims. First, there is a need to quantify the local variations within the trim, and for this purpose, the variations of normalised pressure difference have been considered here (same as in case of [28]). The normalised pressure difference (NPD) has been defined as:

$$\text{NPD} = \frac{P_{\text{in}} - p}{\frac{1}{2} \rho V_{\text{in}}^2} \quad (3)$$

where p and P_{in} are the local and inlet static pressures (in kPa) and V_{in} is the flow velocity magnitude (in m/sec) at the inlet of the flow domain. Variation in normalised pressure difference will help in identifying zones of higher velocity and pressure drop where geometric modification may be necessary. To develop useful design correlations, the parameters need to be presented in non-dimensional form and special care needs to be taken that the equations developed are dimensionally homogeneous [48].

Fig. 9 depicts the variations of normalised pressure difference within a quarter of the baseline trim model. The other quarters of the trim also show the same behaviour and hence are not shown here. It can be seen in the Figure that the normalised pressure difference increases along the flow path from the entry of the trim (row 1) to its exit (row 5). However, this increase in the normalised pressure difference is flow geometry dependent i.e. it is higher in between the cylinders of a particular row, while it is lower at the entry and exit of each row. Lower normalised pressure difference is

noticed just upstream of each cylinder, as expected. It has been found that the average normalised pressure difference at the entry of row 1 is 3.7, while at its exit is 13.6. For row 2, the average normalised pressure difference at the entry will remain the same as on the exit of row 1 i.e. 13.6, while at its exit, it is 19.4. Similarly, at the exits of rows 3, 4 and 5, the average normalised pressure difference values are 29.7, 35.5 and 40.7. These results show that the average normalised pressure difference across row 1 is 13.6–3.7 = 9.9, while for rows 2 to 5 these values are 5.8, 10.3, 5.8 and 5.2 respectively. Upon careful analysis of these results, it can be clearly noticed that although the average normalised pressure difference decreases from row 1 to row 2; it increases from row 2 to row 3. From row 3 to row 4 and from row 4 to row 5, the decreasing trend in the average normalised pressure difference can be seen again. This suggests that the pressure losses in the 3rd row of the trim are significantly higher compared to any other row. However, a more robust quantitative parameter is required to quantify the local pressure losses within the trim.

Based on the above discussions, a dimensionless parameter has been developed that can quantify the local pressure losses, per unit radial distance within the trims. The parameter developed in the present study quantifies the local pressure drop within the trim, and can be represented as:

$$\text{Dpr} = \frac{p_i - p_{i+1}}{r_i - r_{i+1}} \quad (4)$$

where p_i is the local average static pressure (in kPa) upstream of the i th row of the trim, while r_i is the radius (in m), from the centre of the trim, to the location where p_i has been measured. This parameter represents the rate of change in local static pressure with respect to the radius corresponding to each row. This is an important parameter as proper selection of this parameters will ensure gradual change in pressure and will help in avoiding conditions such as cavitation and flashing. Here, $p_i - p_{i+1}$ is the change in local static pressure across a row while $r_i - r_{i+1}$ denotes the change in the radius across the row. The variations in Dpr (in kPa/m) for the baseline model of the trim are depicted in Fig. 10. The variations in Dpr have been plotted against r_i/r_{out} where r_{out} is outer radius of the trim (in m). It can be seen that the value of Dpr across the 1st row is 1787 kPa/m, which decreases to 1428 kPa/m across the 2nd row. This means that although there is a significant pressure drop across the second row of the trim, the rate of pressure drop decrease has reduced by 20%. Across the row 3 of the trim, Dpr value is 3091 kPa/m, which is 116% higher than that across the row 2, and 72.9% higher than that for the row 1. Hence, the pressure drop within the 3rd row of the trim is significantly higher than across the preceding two rows of the trim. Now, across the row 4, the value of Dpr is 2232 kPa/m and across the row 5, Dpr is 2355 kPa/m. The rate of pressure drop across the last row of the trim is slightly higher than that across the row 4 because there are no more rows available after row 5, causing the pressure to further decrease at the exit of the trim.

In order to further analyse the local flow structure within the trim, and to analyse the effect of row 3 in further detail, flow velocity variations within a quarter of the baseline trim are shown in Fig. 11. Fig. 11 depicts the three components of flow velocity in polar coordinates i.e. radial, tangential and axial. All the three velocity components are shown here to analyse the complexity in the local flow fields associated with the trim, and to establish that it is indeed very important to consider the local flow behaviour in the design of a multi-stage continuous-resistance trim. It may be possible to develop an integrated flow model for flow through a complex geometry by combining several local flow models [49]. It can be seen that the radial flow velocity is higher in between the

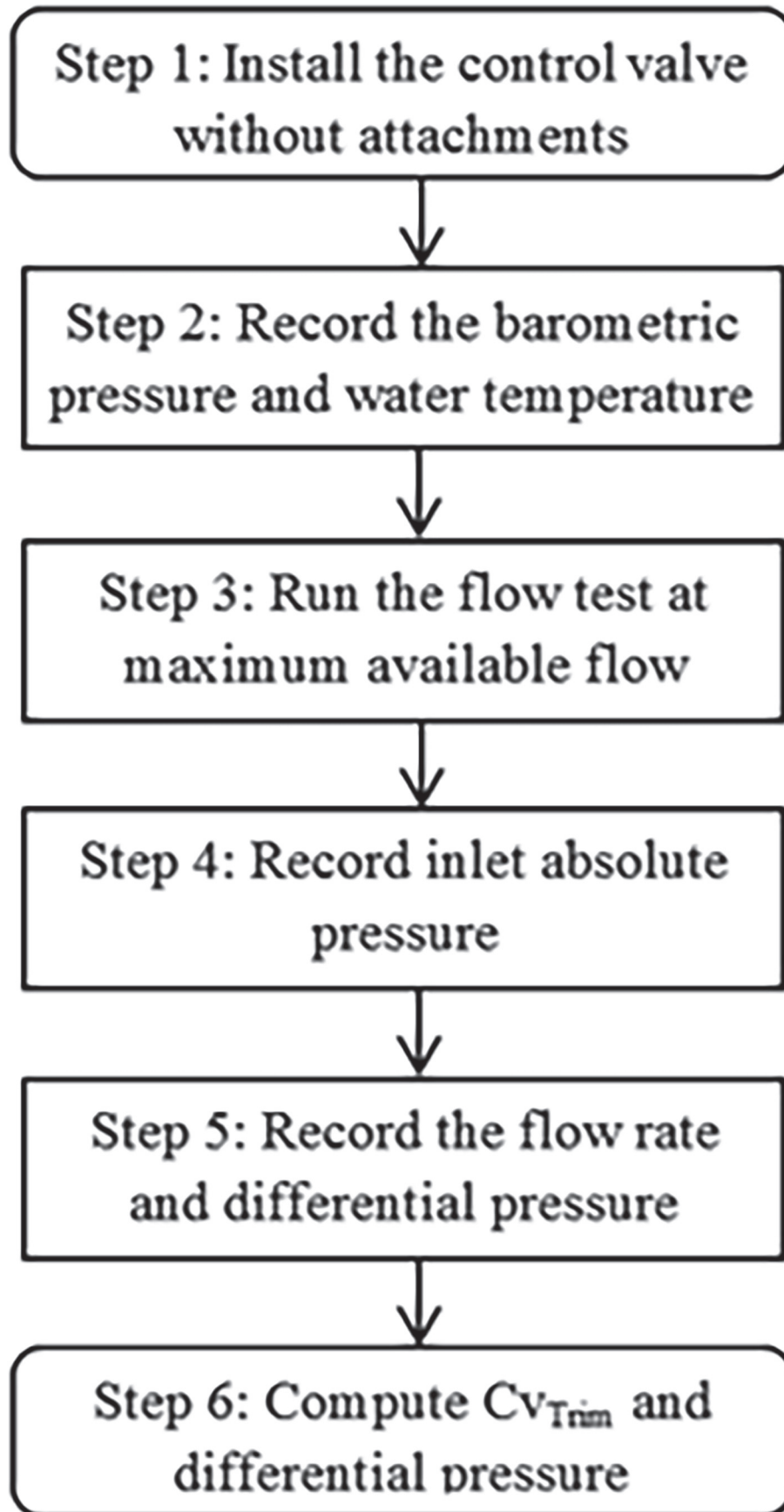


Fig. 8. Flow chart showing the experimental procedure.

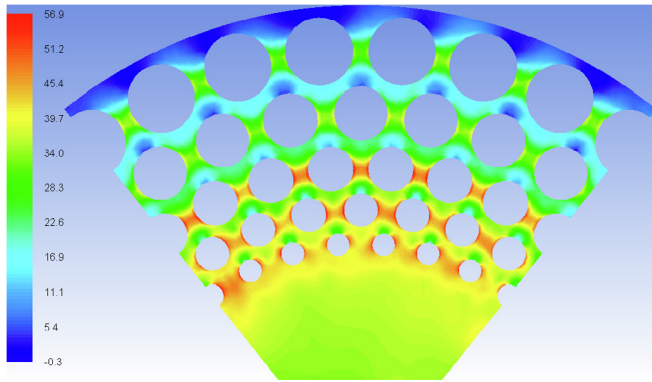


Fig. 9. Variations of normalised pressure drop within the baseline trim.

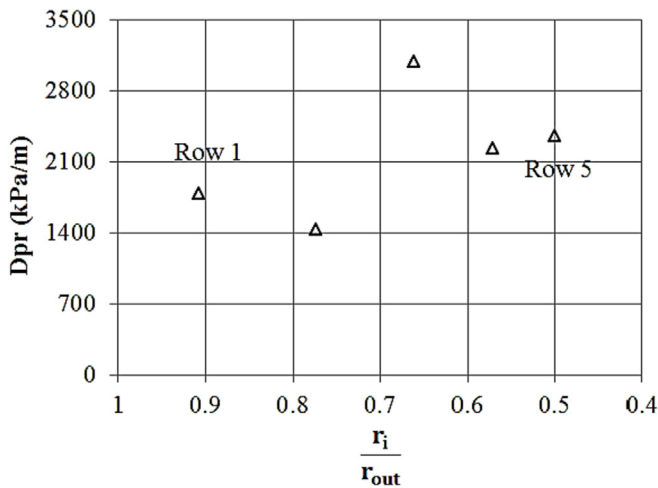


Fig. 10. Variations in rate of pressure loss across the different rows of the baseline trim.

cylinders, while it is lower at the entry and the exit of rows. This trend is valid for all the rows of the trim, however, severe non-uniformities have been observed in the vicinity of cylinders in the 5th row. Moreover, it can be noticed that the highest radial flow velocity is recorded in between the cylinders of the row 3 with the radial velocity values reaching up to 9.79 m/sec. In comparison with the row 3, radial velocity in the row 1 is, on average, 13% lower than that in the row 3. Similarly, the rows 2, 4 and 5 depict radial flow velocities that are 21%, 28% and 49% lower than that in the row 3 respectively. An obvious similarity between the radial flow velocity variations and the normalised pressure drop variations (Fig. 9) is the fact that wherever the radial flow velocity is high, the normalised pressure drop is also high; both these flow parameters are high in between the cylinders of each row. Moreover, as the radial flow velocity is highest in the 3rd row of the trim, the normalised pressure drop is also highest in the 3rd row.

The tangential velocity component within the trim can be seen to be quite systematic in the inner rows of the trim i.e. rows 2, 3 and 4. As the flow has to take place around the cylinders, the tangential flow velocity is higher upstream of the cylinders where flow diversion takes place. Moreover, the tangential velocity component is observed to increase with decreasing radius of the trim. It should be noted here that the primary flow velocity component in this type of trim is the radial component, which dictates the flow behaviour in between the cylinders of a particular row. The axial flow velocity component is very small, with highest axial velocity reaching 2.12 m/sec, which is only 21% of the highest radial flow

velocity and 34% of the highest tangential flow velocity recorded within the trim.

Hence, it has been established that the local flow behaviour within a multi-stage continuous-resistance trim is indeed very complex in nature, and there is a need to integrate local flow characteristics with global performance indicators to have an appropriate design of the trim.

6. Hydrodynamic characterisation of the trim

Both the global performance indicators and the local flow behaviour within a multi-stage continuous-resistance trim are significantly affected by the trim's geometrical features, as indicated in Refs. [21–28]. In order to establish the relationship between the geometrical and hydrodynamic characteristics of the trim, Design of Experiments (DoE) based approach has been used in the present study [50]. In the baseline model of the trim (as in Fig. 2(c)), it can be seen that the diameters of the cylinders of rows 1 to 5 are represented as d_1 , d_2 , d_3 , d_4 and d_5 . Hence, the number of factors involved in DoE is five. Moreover, five levels of each diameter have been considered in the present study to cover a wide range of design possibilities. These levels are referred to as d , $0.95d$, $0.9d$, $0.85d$ and $0.8d$, based on the limitations in the manufacturing of such trims. As the number of parameters and levels considered in the present study are five each, the L25 (5^5) Taguchi's Orthogonal Array (OA) has been developed in order to establish the effects of size of the cylinders of the trim [51]. Hence, the total number of numerical simulations that have been conducted is 25 with varying combinations of the diameters of the cylinders. Table 5 summarises the factors and levels combination. Numerical simulations, using CFD based techniques, have been carried out on all the designs identified.

The pressure drop across each row of cylinders is recorded for each of these simulations. Based on these pressure drop values, the Taguchi design analysis has been carried out. The methodology adopted for this type of analysis is known as Smaller is Better. In this approach, the Signal-to-Noise ratio (S/N) is evaluated for each combination of the factors and levels. The S/N ratio used can be expressed as:

$$\frac{S}{N} = -10 \log_{10} \sum \frac{\Delta P^2}{n} \quad (5)$$

where n is the number of responses of factor-level combinations. The results of this analysis are presented in Fig. 12. The X-axis represents the values of the different factors considered, while the Y-axis represents the mean of the means of ΔP for each row of the trim (in kPa). It can be seen that as the diameter of the cylinders increases, the pressure drop increases, as expected. However, the increase in the pressure drop is maximum in case of row 3. This means that as the diameter of the cylinders of row 3 increases, the pressure drop increase is more severe than in other rows of the trim. Row 1 follows row 3 in this severity, which is then followed by row 4, row 2 and then row 5. It must be noted that the severity of pressure drop increase shown for row 4 is partly due to the effects of row 3. As the flow strikes row 1 first, it is expected to result in higher pressure drop, while at the exit of the trim (row 5), the pressure drop is expected to be much lower as there are no further rows available, and the flow enters the valve body again (with greater area available for the flow to take place).

Based on these results, it can be concluded that the geometrical characteristics of the multi-stage continuous-resistance trim in general, and its 3rd row's geometrical features in specific, significantly affects the hydrodynamic characteristics of the trim. This means that the 3rd row of the trim needs to have its geometrical

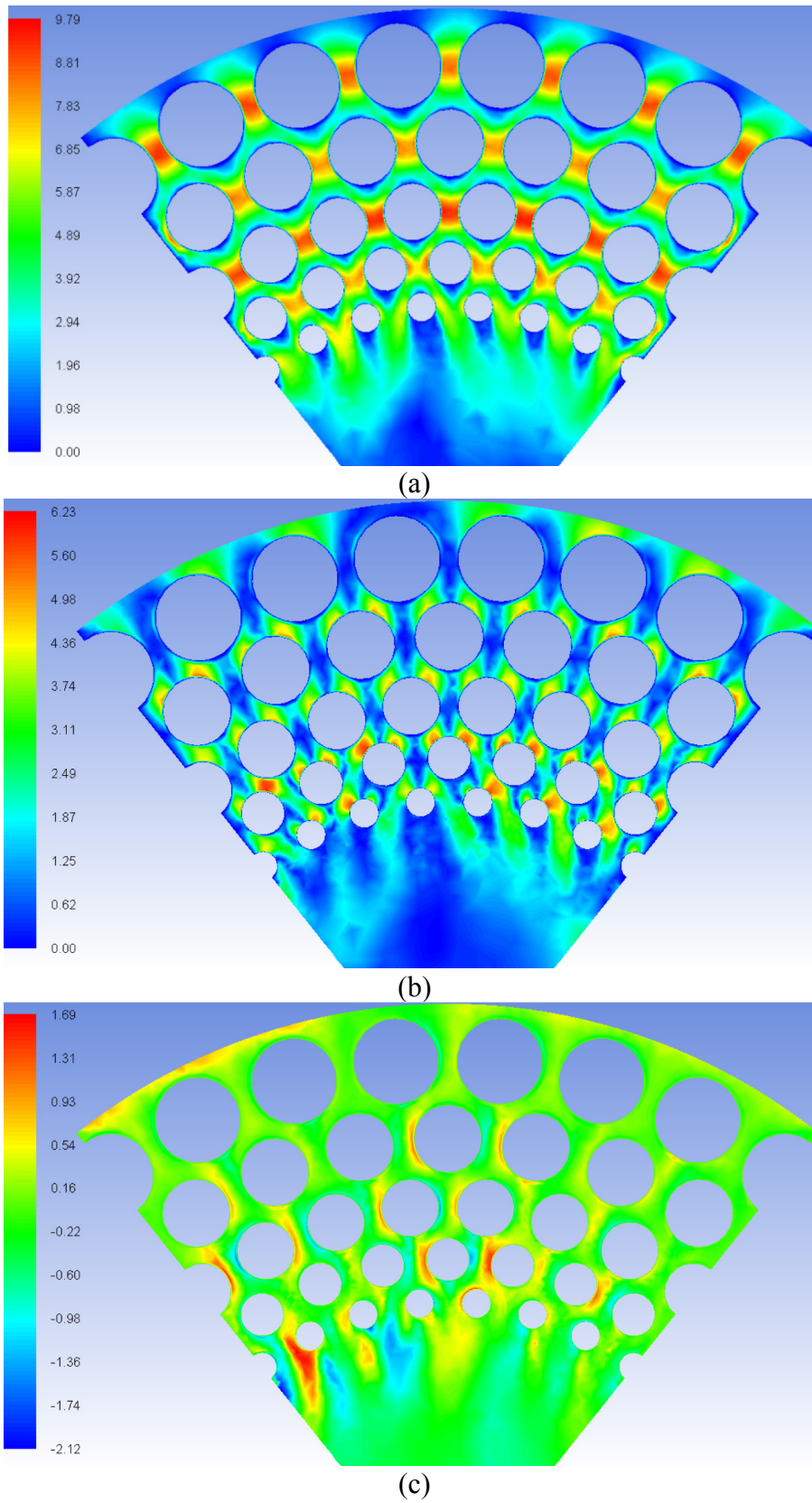


Fig. 11. Variations in flow velocity components of the baseline trim design (a) radial (b) tangential (c) axial.

Table 5
Design of experiments.

d ₁	d ₂	d ₃	d ₄	d ₅
Diameter of cylinders of row 1	Diameter of cylinders of row 2	Diameter of cylinders of row 3	Diameter of cylinders of row 4	Diameter of cylinders of row 5
d ₁	0.95d ₂	0.95d ₃	0.95d ₄	0.95d ₅
d ₁	0.9d ₂	0.9d ₃	0.9d ₄	0.9d ₅
d ₁	0.85d ₂	0.85d ₃	0.85d ₄	0.85d ₅
d ₁	0.8d ₂	0.8d ₃	0.8d ₄	0.8d ₅
0.95d ₁	d ₂	0.95d ₃	0.9d ₄	0.85d ₅
0.95d ₁	0.95d ₂	0.9d ₃	0.85d ₄	0.8d ₅
0.95d ₁	0.9d ₂	0.85d ₃	0.8d ₄	d ₅
0.95d ₁	0.85d ₂	0.8d ₃	d ₄	0.95d ₅
0.95d ₁	0.8d ₂	d ₃	0.95d ₄	0.9d ₅
0.9d ₁	d ₂	0.9d ₃	0.8d ₄	0.95d ₅
0.9d ₁	0.95d ₂	0.85d ₃	d ₄	0.9d ₅
0.9d ₁	0.9d ₂	0.8d ₃	0.95d ₄	0.85d ₅
0.9d ₁	0.85d ₂	d ₃	0.9d ₄	0.8d ₅
0.9d ₁	0.8d ₂	0.95d ₃	0.85d ₄	d ₅
0.85d ₁	d ₂	0.85d ₃	0.95d ₄	0.8d ₅
0.85d ₁	0.95d ₂	0.8d ₃	0.9d ₄	d ₅
0.85d ₁	0.9d ₂	d ₃	0.85d ₄	0.95d ₅
0.85d ₁	0.85d ₂	0.95d ₃	0.8d ₄	0.9d ₅
0.85d ₁	0.8d ₂	0.9d ₃	d ₄	0.85d ₅
0.8d ₁	d ₂	0.8d ₃	0.85d ₄	0.9d ₅
0.8d ₁	0.95d ₂	d ₃	0.8d ₄	0.85d ₅
0.8d ₁	0.9d ₂	0.95d ₃	d ₄	0.8d ₅
0.8d ₁	0.85d ₂	0.9d ₃	0.95d ₄	d ₅
0.8d ₁	0.8d ₂	0.85d ₃	0.9d ₄	0.95d ₅

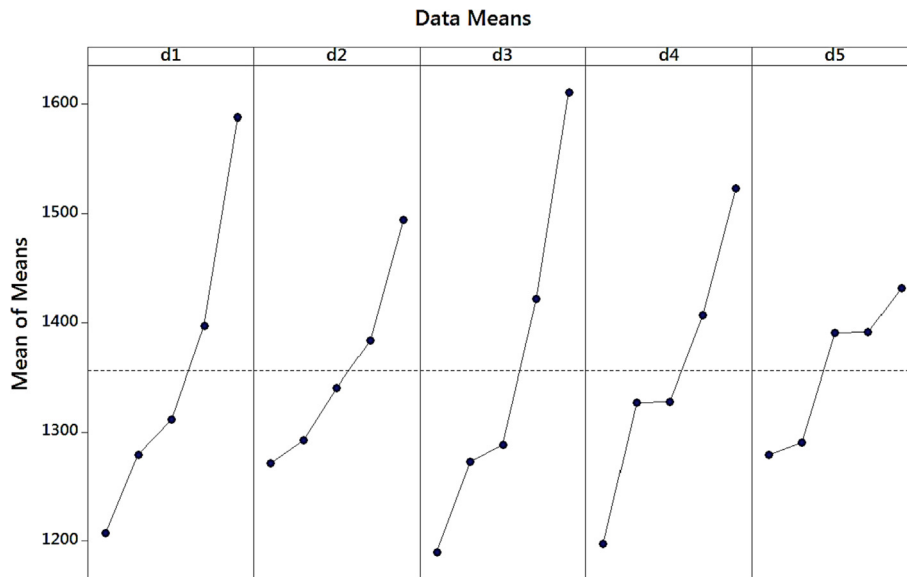


Fig. 12. Variations in the mean pressure drop across the rows of the trim as a function of cylinders' size.

features reviewed/modified in order to enhance the performance of the trim. Moreover, due to manufacturing constraints, the geometrical characteristics of row 1 cannot be modified. It is thus strongly suggested that the geometrical features of a multi-stage continuous-resistance trim be determined and integrated in the design of such trims.

7. Improved design of a multi-stage trim

As it has been identified that the 3rd row of the trim is associated with significant pressure losses within the trim, and that the size of the cylinders within a row has considerable impact on the hydrodynamic characteristics of the trim, the size of the cylinders in different rows need to be modified for an improved trim design.

In order to change the size of the cylinders, the flow areas within the different rows of the trim need to be analysed in detail. Hence, a parameter has been developed (Flow Area Ratio (FAR)), which can be defined as:

$$FAR = \frac{FA_{i+1}}{FA_i} \tag{6}$$

where FA_i is the available flow area (in m²) in the ith row of the trim. Hence, Flow Area Ratio defined in equation (6) is the ratio of the available flow areas within consecutive rows of the trim. The FAR can be an important parameter for the design as once the outlet area of the trim has been specified; appropriate FAR values can be used to provide flow areas corresponding to different flow paths.

The variations in FAR for the baseline trim model are shown in Fig. 13. The variations in FAR have been plotted against the centre point distance between two consecutive rows of the trim. As discussed earlier, cylinders based multi-stage trims are designed based on gradual flow area expansion from the inlet to the outlet i.e. from the outer most row to the inner most row in the present study. This means that FAR from row 1 to row 5 should always be higher than 1. It can be clearly seen that this is not the case between the 2nd and the 3rd rows, where instead of an FAR between 1.13 and 1.21, it is actually 0.89. This suggests that in the baseline trim model, there is area contraction from the row 2 to the row 3. This increases the pressure losses within the row 3, associated with higher flow velocities seen earlier. From the rows 3 to 4 and the rows 4 to 5, the usual area expansion trends can be seen. Thus, for an improved design of a cylinders based multi-stage trim, the FAR should be adjusted such that each preceding row should offer area expansion in a systematic manner.

Fig. 14 depicts the Flow Area Ratio variations that have been selected for the improved trim model. It can be seen that the FAR value between the first 2 rows of the trim remains the same as in the case of baseline trim model (i.e. 1.13). This is because these two rows were offering area expansion. The FAR value between rows 2 and 3 has been computed based on an area ratio of $(1.13 + 1.21) / 2 = 1.17$. The modified FAR between rows 2 and 3 is thus 31.7% higher than in the baseline trim model. Similarly, keeping the FAR values between rows 3 and 4 and between rows 4 and 5 the same as in the baseline trim model, the modified Flow Area (FA) values have been computed, which are 32.7% and 32.4% higher than in the baseline trim model respectively. Thus, it is expected that the improved trim design would offer continuous area expansion to the flow, hence, reducing the losses within the trim.

Based on the FAR calculations presented above, the improved design of the trim has been created. The geometrical details of the improved trim model are summarised in Table 6. It can be seen that the sizes of row 1 and row 2 cylinders (i.e. d_1 and d_2) remain the same as in the case of the baseline trim model, however, the cylinders in rows 3 to 5 are smaller in size in the improved trim. The reduction in cylinder size for row 3 is about 11% compared to the baseline trim. Similarly, the size reductions in rows 4 and 5 are about 17% and 33% respectively.

The improved trim design has then been numerically tested using CFD based techniques discussed earlier, for the same boundary and operating conditions. The normalised pressure difference and velocity components' variations are recorded for the

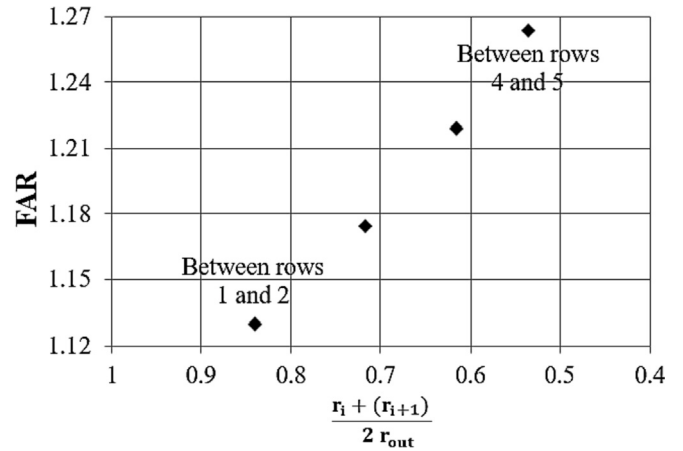


Fig. 14. Flow Area Ratio variations within the improved trim model.

Table 6
Cylinder sizes of the improved trim design.

Improved trim design	Value
Diameter of cylinders of row 1	d_1
Diameter of cylinders of row 2	d_2
Diameter of cylinders of row 3	$0.89d_3$
Diameter of cylinders of row 4	$0.83d_4$
Diameter of cylinders of row 5	$0.67d_5$

improved trim, and the results have been compared against the baseline trim results. Fig. 15 depicts the variations of normalised pressure difference within the improved trim model. The scale of the contour has been kept the same as in case of the baseline model (Fig. 9) for effective comparison purposes. The most obvious point that can be noted is that the normalised pressure difference values across the whole trim are much lower than for the baseline trim. It has been evaluated that the average normalised pressure difference at the entry of row 1 is 1.9, which is 47.6% lower than for the baseline trim model. At the exit of row 1, the average normalised pressure difference is 11.1, which is 18% less than for the baseline model. Similarly, at the exits of rows 2, 3, 4 and 5, the average normalised pressure difference values are 19.4%, 34.3%, 33.8% and 36.6% less than for the baseline trim. Hence, it can be concluded that the losses within the improved trim model are significantly reduced in comparison with the baseline trim model.

The parameter that was used to quantify the pressure drop within the baseline trim model (i.e. D_{pr}) has also been used to test the appropriateness of the improved trim design. A comparison of

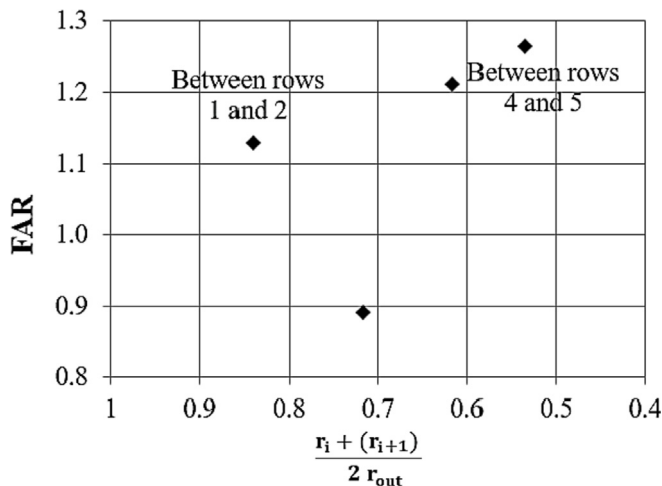


Fig. 13. Flow Area Ratio variations within the baseline trim model.

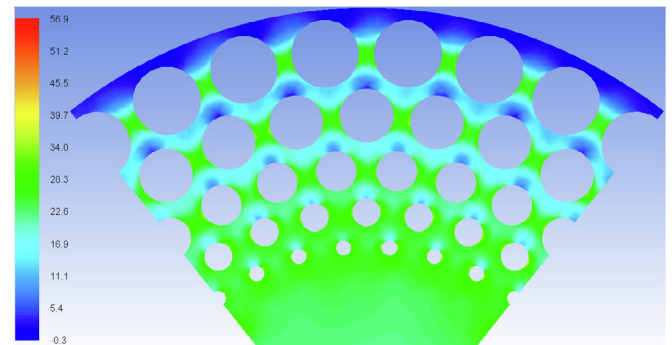


Fig. 15. Variations of normalised pressure drop within the improved trim.

this parameter for the two trim models considered here (baseline and the improved) is shown in Fig. 16. It can be clearly seen that the pressure losses within row 3 of the trim have now decreased significantly. The decrease in the rate of pressure drop within the improved trim model, in comparison with the baseline trim model, for rows 1 to 5, are 6.3%, 22.3%, 62.5%, 31.2% and 55.5% respectively. The reduction in the rate of pressure drop across rows 1 and 2 suggest that row 3 also affects (to some extent) the hydrodynamic characteristics of rows 1 and 2, which was not evident while analysing the baseline trim earlier. Hence, a comparison of the rate of pressure drop across the different rows of the trims is an effective tool that can be utilised for the characterisation of the hydrodynamic behaviour of trims. Another indication from Fig. 16 is that the effect of row 3 on row 4 is more pronounced. Based on the area ratio calculations, it was expected that Dpr would continuously decrease from row 1 to row 5, however, it can be seen that the rate of pressure drop in row 4 is still higher than row 3. This further implies that Dpr needs to be used in an iterative manner in order to optimally design these multi-stage trims, for minimum pressure drop across the trims.

Fig. 17 depicts the flow velocity components in polar coordinates within the improved trim. In comparison with Fig. 11, it can be seen that both the radial and tangential velocities are significantly lower in the improved trim model. The axial velocity component, as mentioned earlier for the baseline trim model, is too small to affect the performance of the trim. In comparison with the baseline trim model, the average radial flow velocity in between the cylinders of row 1 of the improved trim is 7.3% less. Similarly, for rows 2 to 5, the average radial flow velocities in between the cylinders are 10.9%, 40.8%, 39.1% and 36% lower than for the baseline trim. Again, it can be seen that the radial flow velocity in the row 4 is slightly higher than expected, because of the aforementioned reasons.

As a concept design, it has been shown numerically that the improved trim design performs hydrodynamically better than the baseline trim model. However, this concept design needs to be proven experimentally. Hence, the improved trim model was manufactured using the same material and tolerances, and tested in the same flow loop with the same operating conditions. The improved trim model is shown in Fig. 18. The pressure drop across the control valve, installed with the improved trim model, has been experimentally obtained to be 168 kPa, which is considerably less than 184.9 kPa as obtained for the baseline trim model. Hence, a 9.1% reduction in the pressure drop, across the control valve has

been achieved, ensuring that the improved trim design is indeed efficient, and hence, the multi-stage continuous-resistance trim design developed here, based on flow area ratio, is more accurate in achieving the desired global performance indicators.

8. Energy loss analysis of the trim

In order to ascertain the hydrodynamic efficiency of the improved trim, over the baseline trim, a parameter has been developed to determine the energy efficiency of both the trims. This parameter (DE) is representative of the change of energy across the different rows of both the trim models. The parameter DE can be expressed as:

$$DE = \frac{(P_i - P_{i+1})}{\rho g} + \frac{V_i^2 - V_{i+1}^2}{2g} \quad (7)$$

where V_i is the average flow velocity magnitude upstream the i th row of the trim (in m/sec), ρ is the density of water (in kg/m³) and g is the gravitational acceleration (in m/sec²). In equation (7), $V_i - V_{i+1}$ denotes the change in average local flow velocity magnitude across a row of the trim. The variations in DE (in m), across the different rows of both the trim models, have been shown in Fig. 19, where r_{out} is the outer radius of the trim (in m). It can be seen that the energy losses across the different rows of the improved trim model are significantly lower than for the baseline trim model. The reduction in energy losses, across the 3rd row of the improved trim is 55.7%. Moreover, energy losses across rows 1, 2, 4 and 5 of the improved trim are 18.2%, 4%, 41.1% and 67.7% lower than for the baseline trim. Hence, on average, the energy losses across the improved trim are 37.9% lower than the baseline trim. This means that the improved trim is 37.9% more energy efficient than the baseline trim. This further ascertains that the trim design developed here, based on FAR, is superior to the existing design that does not consider geometric features and local flow behaviour explicitly.

9. Conclusions

The hydrodynamic characteristics of multi-stage continuous-resistance control valve trims are significantly influenced by the local geometric/design features of the trim. These features include size and location of cylinders embedded within the disks to create desired flow paths. The current design and analysis methodology for these trims do not explicitly take into account the interrelation between the geometric/design features and the corresponding local flow behaviour, resulting in inefficient trim designs. In the current study an explicit interrelationship has been established between these parameters. The main conclusions that can be drawn from this work are:

- There are significant non-uniformities observed in local pressure and flow velocity fields within multi-stage continuous-resistance trims because of local geometric/design features. It has been seen that location and the size of cylinders affect the local flow fields, and hence the overall energy loss through the trims. Through optimal selection of the size and location of these cylinders, the non-uniformities can be managed in order to develop more efficient trim designs with improved hydrodynamic characteristics and longer life span.
- The geometrical characteristics of a multi-stage continuous-resistance trim substantially affect the hydrodynamic behaviour of the trim. In poorly designed trims, it has been shown that the inherent local pressure drop variations do not conform to the trim's design philosophy. Hence, local maximas in pressure drop

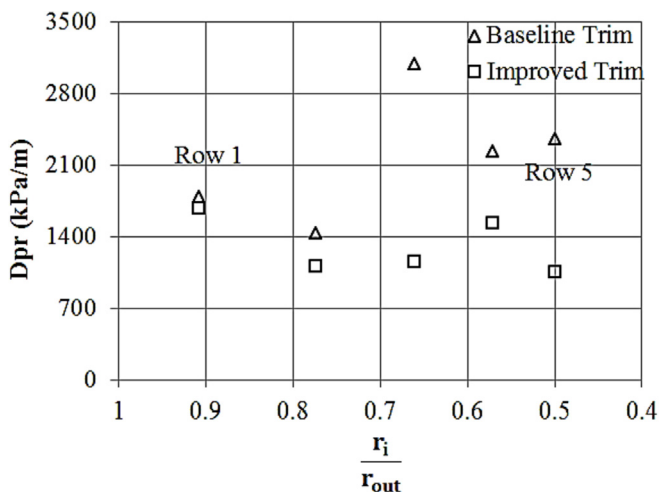


Fig. 16. Comparison of pressure loss across the different rows of the baseline and the improved trims.

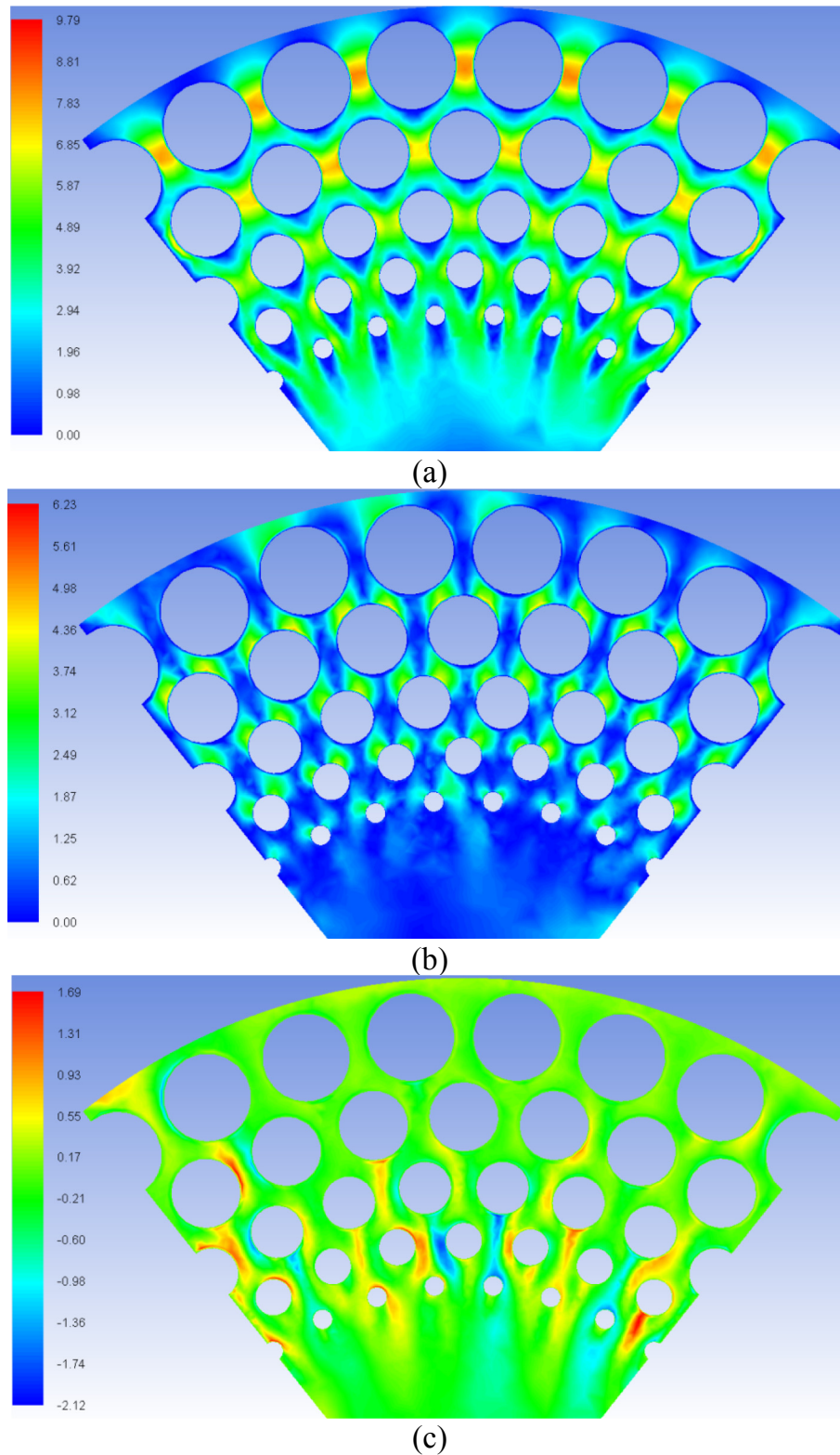


Fig. 17. Variations in flow velocity components of the improved trim design (a) radial (b) tangential (c) axial.

and flow velocity have been observed, which are indicative of likelihood of cavitation and flashing.

- A novel geometry based design parameter (Flow Area Ratio, FAR) has been developed that uniquely defines the flow area change in the flow path corresponding to each row of the trim. It

thus enables easy quantification of the effects of change in flow area on the local flow features, and hence on the hydrodynamic characteristics of the trim. FAR has thus been used as a design parameter to design flow paths in a trim enabling desired control over local flow features. It has been shown that poorly

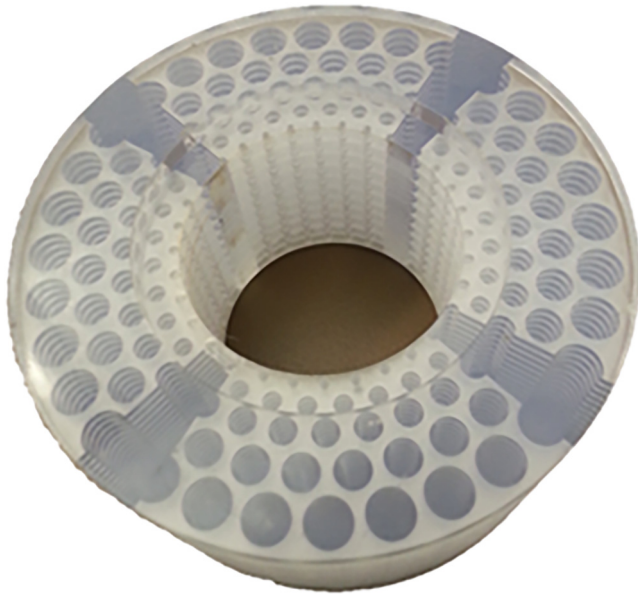


Fig. 18. The improved trim design.

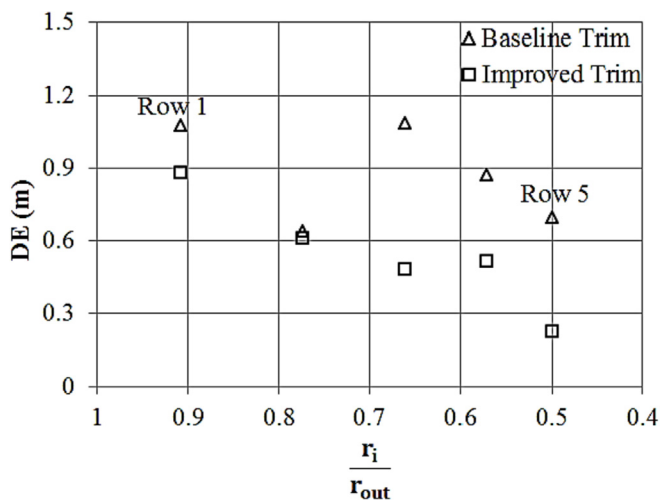


Fig. 19. Comparison of energy loss across the different rows of the baseline and the improved trims.

designed trim doesn't exhibit systematic variations in FAR. This parameter has then been used to rectify the design flaws of the trim. In general, FAR can be used for more efficient trim designs.

- Control valves are often used in processing plants and contribute to overall energy loss in the system. An over/under sized valve trim will compound this problem by causing additional energy losses. The trim and associated flow paths need to be appropriately designed to minimise energy loss through the trim. In the present study, a new/improved trim has been designed in order to enhance the hydrodynamic characteristics of the trim. The new trim design has been shown to be 37.9% more energy efficient than the baseline trim design.

It is thus clear that the improved design, which takes into account the local flow behaviour within the trim, and the trim's geometrical features, is more efficient compared to the existing trim design. However, this study can be extended further by analysing different trim designs, such as discrete trims (labyrinth) etc.

Nomenclature

c	Numerical constant (–)
CV_{Seat}	Flow capacity of the seat ($\sqrt{m^7/kg}$)
CV_{Body}	Flow capacity of the valve body ($\sqrt{m^7/kg}$)
CV_{Trim}	Flow capacity of the trim ($\sqrt{m^7/kg}$)
$CV_{Control-Valve}$	Flow capacity of the control valve ($\sqrt{m^7/kg}$)
d	Diameter of cylinders (m)
D	Diameter of pipeline (m)
D_{pr}	Pressure loss parameter (kPa/m)
DE	Energy loss parameter (m)
FA_i	Flow area available in the i th row of the trim (m^2)
FAR	Flow Area Ratio (–)
g	Gravitational Acceleration (m/sec^2)
n	Number of responses (–)
p	Local static gauge pressure (kPa)
P_i	Average static pressure upstream the i th row of the trim (kPa)
P_{in}	Static gauge pressure at the inlet boundary of the flow domain (kPa)
ΔP_{Trim}	Differential pressure across the trim (kPa)
$\Delta P_{Control-Valve}$	Differential pressure across the control valve (kPa)
Q_{Trim}	Volumetric flow rate passing through the trim (m^3/hr)
$Q_{Control-Valve}$	Volumetric flow rate passing through the control valve (m^3/hr)
r	Radius of rows (m)
r_i	Radius upstream the i th row of the trim (m)
r_{out}	Outer radius of the trim (m)
V_i	Average flow velocity magnitude upstream the i th row of the trim (m/sec)
V_{in}	Flow velocity magnitude at the inlet of the valve (m/sec)

Greek Symbols

α	Piping geometry factor (–)
γ	Reynolds number factor (–)
k	Turbulent kinetic energy (m^2/sec^2)
ω	Turbulent dissipation rate ($1/sec$)
ρ	Density of the fluid (kg/m^3)
ρ_o	Operating density (kg/m^3)

Abbreviations

CFD	Computational Fluid Dynamics
DoE	Design of Experiments
GCS	Grid Convergence Study
OA	Orthogonal Array
POD	Proper Orthogonal Decomposition
PVC	Polyvinyl Chloride
RANS	Reynolds averaged Navier-Stokes
RNG	Re-Normalisation Group
SIMPLE	Semi Implicit Method for Pressure Linked Equations
SST	Shear Stress Transport
S/N	Signal-to-Noise Ratio

References

- Industrial process control valves, Part 1: control valve terminology and general considerations. British Standards BSI; 2005. BS EN 60534-1.
- Industrial process control valves, Part 2-1: flow capacity – sizing equations for fluid flow under installed conditions. British Standards BSI; 2011. BS EN 60534-2-1.
- Singleton EW. A specifier's guide to control valves. KCI Publishing; 2013.
- Singleton EW. The role of the control valve in improved process control, ABB Control Valves. 1999. reprinted from Valve World (4).
- Le QD, Mereu R, Besagni G, Dossena V, Inzoli F. Computational fluid dynamics modelling of flashing flow in convergent–divergent nozzle. Am Soc Mech Eng: J Fluids Eng 2018;140:101102.
- Liao Y, Lucas D. 3D CFD simulation of flashing flows in a converging-diverging nozzle. Nucl Eng Des 2015;292:149–63.

- [7] Giacomelli F, Biferi G, Mazzelli F, Milazzo A. CFD modeling of the supersonic condensation inside a steam ejector. *Energy Proc* 2016;101:1224–31.
- [8] Oil, Gas and Petroleum Equipment. Enhanced cage guided control valves unveiled. 2017. accessible online at, <https://www.ogpe.com/articles/print/volume-64/issue-1/downstream/enhanced-cage-guided-control-valves-unveiled.html>.
- [9] Industrial process control valves, Part 2-3: flow capacity – test procedures. British Standards BSI; 1998. BS EN 60534-2-3.
- [10] Industrial process control valves, Part 2-4: flow capacity – inherent flow characteristics and rangeability. British Standards BSI; 2003. BS EN 60534-2-4.
- [11] Industrial process control valves, Part 2-5: flow capacity – sizing equations for fluid flow through multistage control valves with interstage recovery. British Standards BSI; 2009. BS EN 60534-2-5.
- [12] Green J, Mishra R, Charlton M, Owen R. Validation of CFD predictions using process data obtained from flow through an industrial control valve. *J Phys Conf Ser* 2012;364.
- [13] Green J, Mishra R, Charlton M, Owen R. Local analysis of flow conditions within a geometrically complex control valve trim using CFD. *J Phys Conf Ser* 2012;364.
- [14] Klas R, Haban V, Rudolf P. Study of the nozzle check valve with respect to its operating characteristics. *EPJ Web Conf* 2018;180:02044.
- [15] Asim T, Charlton M, Mishra R. CFD based investigations for the design of control valves used in energy systems. *Energy Convers Manag* 2017;153:288–303.
- [16] Asim T, Mishra R, Charlton M, Oliveira C. Capacity testing and local flow analysis of a geometrically complex trim installed within a commercial control valve, international conference on jets, wakes and separated flows, 16–18 June, Stockholm, Sweden. 2015.
- [17] Oliveira A. Capacity testing of X-Stream valves for single-component single-phase flows. Technical report submitted to. Weir Valves and Controls Ltd; 2017.
- [18] Wang P, Ma H, Quay B, Santavicca DA, Liu Y. Computational fluid dynamics of stream flow in a turbine control valve with a bell-shaped spindle. *Appl Therm Eng* 2018;129:1333–47.
- [19] Qiu T, Dai H, Lei Y, Liu Y. Effects of valve needle speed on flow characteristics in control valve for unit pump fuel system. *Adv Mech Eng* 2018;10:1–10.
- [20] Kong L, Wei W, Yan Q. Application of flow field decomposition and reconstruction in studying and modeling the characteristics of a cartridge valve. *Eng Appl Comput Fluid Mech* 2018;12:385–96.
- [21] Morton K. Optimisation of a high-energy loss control valve trim using computational and experimental techniques. Ph.D. Thesis. U.K: University of Manchester; 2003.
- [22] Asim T. Capacity testing of X-Stream valves for single-component single-phase flows. Technical report submitted to. Weir Valves and Controls Ltd; 2013.
- [23] Charlton M. Cost effective manufacturing and optimal design of X-stream trims for devere service control valves. M.Sc. by U.K: Research Thesis, University of Huddersfield; 2015.
- [24] Charlton M, Asim T, Mishra R. The effect of manufacturing method induced roughness on control valve performance. In: 6th international and 43rd National conference on fluid mechanics and fluid power, 15–17 December. Allahabad, India: MNNIT; 2016.
- [25] Lisowski E, Filo G. CFD analysis of the characteristics of a proportional flow control valve with an innovative opening shape. *Energy Convers Manag* 2016;123:15–28.
- [26] Lisowski E, Filo G, Rajda J. Analysis of flow forces in the initial phase of throttle gap opening in a proportional control valve. *Flow Meas Instrum* 2018;59:157–67.
- [27] Sun X, Kim HS, Yang SD, Kim CK, Yoon JY. Numerical investigation of the effects of surface roughness on the flow coefficient of an eccentric butterfly valve. *J Mech Sci Technol* 2018;31:2839–48.
- [28] Jin ZJ, Gao ZX, Z M, Liu BZ, Qian JY. Computational fluid dynamics analysis on orifice structure inside valve core of pilot-control angle globe valve, Institute of Mechanical Engineers Part C. *J Mech Eng Sci* 2018;232:2419–29.
- [29] Ansys 17.0 user guide Available online at: https://www.sharcnet.ca/Software/Ansys/17.0/en-us/help/flu_ug/flu_ug.html.
- [30] Asim T, Mishra R. Computational fluid dynamics based optimal design of hydraulic capsule pipelines transporting cylindrical capsules. *Int J Powder Technol* 2016;295:180–201.
- [31] Asim T, Mishra R, Abushaala S, Jain A. Development of a design methodology for hydraulic pipelines carrying rectangular capsules. *Int J Press Vessel Pip* 2016;146:111–28.
- [32] Asim T, Mishra R. Effect of capsule shape on hydrodynamic characteristics and optimal design of hydraulic capsule pipelines. *J Pet Sci Eng* 2018;161:390–408.
- [33] Versteeg HK, Malalasekera W. An introduction to computational fluid dynamics. U.K: Longman Scientific and Technical; 1995. ISBN 0131274988.
- [34] Pozrikidis C. Fluid dynamics theory, computation and numerical simulation. U.S.A: Kluwer Academic Publishers; 2001. ISBN 038795869X.
- [35] Cebeci T, Shao J, Kafyeke F, Laurendeau E. Computational fluid dynamics for engineers. U.S.A: Horizons Publishing; 2005. ISBN 3540244514.
- [36] Blazek J. Computational fluid dynamics principles and applications. Elsevier; 2001. ISBN 0080430090.
- [37] Asim T, Mishra R. Optimal design of hydraulic capsule pipelines transporting spherical capsules. *Can J Chem Eng* 2016;94:966–79.
- [38] Asim T. Computational fluid dynamics based diagnostics and optimal design of hydraulic capsule pipelines. Ph.D. Thesis. U.K: University of Huddersfield Huddersfield; 2013.
- [39] Menter FR. Two-equation eddy-viscosity turbulence models for engineering applications. *Am Inst Aeronaut Astronaut* 1994;32:1598–605.
- [40] Pradhan S, Mishra R, Ubbi K, Asim T. Optimal design of a four-sensor probe system to measure the flow properties of the dispersed phase in bubbly air-water multiphase flows. *Sensor Actuator Phys* 2013;201:10–22.
- [41] Asim T, Mishra R, Kollar LE, Pradhan SR. Optimal sizing and life-cycle cost modelling of pipelines transporting multi-sized solid-liquid mixtures. *Int J Press Vessel Pip* 2013;113:40–8.
- [42] Mishra R, Palmer E, Fieldhouse J. An optimization study of a multiple-row pin-vented brake disc to promote brake cooling using computational fluid dynamics. *Proc Inst Mech Eng - Part D J Automob Eng* 2009;223:865–75.
- [43] Patankar SV, Spalding DB. A calculation procedure for heat, mass and momentum transfer in three-dimensional parabolic flows. *Heat Mass Transf* 1972;15:1787–806.
- [44] Asim T, Mishra R. Large eddy simulation based analysis of complex flow structures within the volute of a vaneless centrifugal pump. *Sadhana* 2017;42:505–16.
- [45] Richardson LF. The approximate arithmetical solution by finite differences of physical problems including differential equations, with an application to the stresses in a masonry dam. *Philos Trans R Soc London, Ser A* 1911;210:307–57.
- [46] Mishra R, Singh SN, Seshadri V. Study of wear characteristics and solid distribution in constant area and erosion-resistant long-radius pipe bends for the flow of multisized particulate slurries. *Wear* 1998;217:297–306.
- [47] Mishra R, Singh SN, Seshadri V. Velocity measurement in solid-liquid flows using an impact probe. *Flow Meas Instrum* 1998;8:157–65.
- [48] Tesfa B, Gu F, Mishra R, Ball A. LHV prediction models and LHV effect on the performance of CI engine running with biodiesel blends. *Energy Convers Manag* 2013;71:217–26.
- [49] Mishra R, Singh SN, Seshadri V. Improved model for the prediction of pressure drop and velocity field in multi-sized particulate slurry flow through horizontal pipes. *Powder Handling Process* 1998;10:279–87.
- [50] Taguchi G. Introduction to quality engineering: designing quality into products and processes. Tokyo, Japan: Asian Productivity Organisation; 1986.
- [51] Taguchi G, Konishi S. Orthogonal arrays and linear graphs: tools for quality engineering. Dearborn, U.S.A: American Supplier Institute Press; 1987.